# Theory of Multichannel Thermal Unimolecular Reactions. 2. Application to the Thermal Dissociation of Formaldehyde

**J. Troe**

*Institut für Physikalische Chemie, Universität Göttingen, Tammannstrasse 6, D-37077 Göttingen, Germany*

*Received: March 1, 2005; In Final Form: July 4, 2005*

The thermal dissociation of formaldehyde proceeds on three channels, the molecular-elimination channel $H_2CO \rightarrow H_2 + CO$ (1), the radical-forming bond-fission channel $H_2CO \rightarrow H + HCO$ (2), and the bond-fission-initiated, intramolecular-hydrogen-abstraction channel $H_2CO \rightarrow H\cdots HCO \rightarrow H_2 + CO$ (3) which also forms molecular products. The kinetics of this system in the low-pressure range of the unimolecular reaction is shown to be governed by a subtle superposition of collisional channel coupling to be treated by solving a master equation, of rotational channel switching accessible through ab initio calculations of the potential as well as spectroscopic and photophysical determinations of the threshold energies and channel branching above the threshold energy for radical formation which can be characterized through formaldehyde photolysis quantum yields as well as classical trajectory calculations. On the basis of the available information, the rate coefficients for the formation of molecular and radical fragments are analyzed and extrapolated over wide ranges of conditions. The modeled rate coefficients in the low-pressure range of the reaction (neglecting tunneling) over the range 1400−3200 K in the bath-gas Ar in this way are represented by $k_{0,Mol}/[Ar] \approx 9.4 \times 10^{-9}$ exp(−33 140 K/*T*) cm$^3$ molecule$^{-1}$ s$^{-1}$ and $k_{0,Rad}/[Ar] \approx 6.2 \times 10^{-9}$ exp(−36 980 K/*T*) cm$^3$ molecule$^{-1}$ s$^{-1}$. The corresponding values for the bath-gas Kr, on which the analysis relies in particular, are $k_{0,Mol}/[Kr] \approx 7.7 \times 10^{-9}$ exp(−33 110 K/*T*) and $k_{0,Rad}/[Kr] \approx 4.1 \times 10^{-9}$ exp(−36 910 K/*T*) cm$^3$ molecule$^{-1}$ s$^{-1}$. While the threshold energy $E_{0,2}$ for channels 2 and 3 is taken from spectroscopic measurements, the threshold energy $E_{0,1}$ for channel 1 is fitted on the basis of experimental ratios $k_{0,Rad}/k_{0,Mol}$ in combination with photolysis quantum yields. The derived value of $E_{0,1}(1) = 81.2$ (±0.9) kcal mol$^{-1}$ is in good agreement with results from recent ab initio calculations, 81.9 (±0.3) kcal mol$^{-1}$, but is higher than earlier results derived from photophysical experiments, 79.2 (±0.8) kcal mol$^{-1}$. Rate coefficients for the high-pressure limit of the reaction are also modeled. The results of the present work markedly depend on the branching ratio between channels 2 and 3. Expressions of this branching ratio from classical trajectory calculations and from photolysis quantum yield measurements were tested. At the same time, a modeling of the photolysis quantum yields was performed. The formaldehyde system so far presents the best characterized multichannel dissociation reaction. It may serve as a prototype for other multichannel dissociation reactions.

## I. Introduction

Thermal unimolecular reactions proceeding on two (or more) competing channels (denoted by *i*) can have unusual properties. The channels are characterized by specific rate constants $k_i(E,J)$ which may have quite different properties, particularly if they involve transition states of different rigidity. Different dependencies of $k_i(E,J)$ on the energy *E* and on the angular momentum (quantum number *J*) may lead to vibrational and rotational "channel switching"; see, for example, ref 1. The branching ratio of the rate coefficients in the high-pressure range of the reaction corresponds to Boltzmann averages over the specific rate constants $k_i(E,J)$ of the channels *i* and, thus, depends on $k_i(E,J)$ in a simple way. In the falloff range and, in particular, in the low-pressure limit of the reaction, however, the $k_i(E,J)$ values are not sampled by Boltzmann but by nonequilibrium populations of excited states. These depend strongly on the character of the collisional energy transfer involved, varying between weak and strong collisions. The rate coefficients, thus, not only reflect the properties of $k_i(E,J)$ but also reflect those of collisional energy transfer, particularly of the ratio $\langle\Delta E\rangle/F_E kT$ which characterizes the efficiency of the collisions ($\langle\Delta E\rangle$ = average total energy transferred per collision and $F_E$ = factor characterizing the energy dependence of the vibrational density of states[2]). In this case, knowledge of the properties of rovibrational energy transfer is required, and two-dimensional (2D) master equations (in the variables *E* and *J*) have to be solved.[2] In the absence of detailed knowledge about rovibrational energy transfer, one might hope that one-dimensional (1D) master equations will capture the essential features of the problem. As the influence of collisions will be the most pronounced in the low-pressure limit of the reaction, one may first focus attention on this range of the reaction and approach the intermediate falloff and the high-pressure range only after the low-pressure limit is well understood.

For the low-pressure limit, the master equation can be solved relatively easily. It can even be obtained in analytical form[2] if an exponential collision model is employed. Since the results of detailed experimental studies of energy transfer were very similar to exponential collision models,[3−6] the analytical solutions of the master equation for exponential models from ref 2 appear sufficiently realistic and adequate for many practical purposes. We have implemented these solutions, for example, into a treatment of two-channel thermal unimolecular reactions in part 1 of this series.[7] It was shown that the upper of the two channels, in the case of weak collisions and in the low-pressure

10.1021/jp051027d CCC: $30.25 
Published on Web 08/24/2005

**TABLE 1: Experimental Low Pressure Rate Coefficients $k_{0,Mol}$ (channels 1 + 3) and $k_{0,Rad}$ (channel 2) for the Pyrolysis of Formaldehyde in M = Ar and Kr**

| $k_0$/[M] cm$^3$ molecule$^{-1}$ s$^{-1}$ | reaction | $T$/K | M | P/bar | reference |
|---|---|---|---|---|---|
| $5.25 \times 10^{-9}$ exp(−37 700/$T$) | (2) | 2200−2650 | Ar | 1.0−2.0 | Saito et al. (1985)[13] |
| $3.4 \times 10^{-17}$ | | 2000 | | | |
| $2.08 \times 10^{-8}$ exp(−39 170/$T$) | (2) | 1650−2200 | Ar | 1.5−2.5 | Rimpel and Just (1988)[14] |
| $6.5 \times 10^{-17}$ | | 2000 | | | |
| $5.18 \times 10^{-10}$ exp(−28 100/$T$) | (1) + (3) | 1900−2400 | | | |
| $4.1 \times 10^{-16}$ | | 2000 | | | |
| $2.7 \times 10^{12}$ T$^{-5.54}$ exp(−48660/$T$) | (2) | 1700−3200 | Kr | 0.4−1.1 | Irdam et al. (1992)[15] |
| $3.8 \times 10^{-17}$ | | 2000 | | | |
| $9.2 \times 10^{-9}$ exp(−37 750/$T$) | (2) | 1400−2000 | Ar | 1.4−2.5 | Hidaka et al. (1993)[16] |
| $5.8 \times 10^{-17}$ | | 2000 | | | |
| $1.02 \times 10^{-8}$ exp(−38 706/$T$) | (2) | 2004−2367 | Kr | 0.2−0.4 | Kumaran et al. (1998)[17] |
| $4.0 \times 10^{-17}$ | | 2000 | | | |
| $4.66 \times 10^{-9}$ exp(−31 210/$T$) | (1) + (3) | 2004−2367 | | | |
| $5.0 \times 10^{-16}$ | | 2000 | | | |
| $8.30 \times 10^{-9}$ exp(−37 044/$T$) | (2) | 1675−2080 | Ar | 1.2 | Friedrichs et al. (2004)[19] |
| $7.5 \times 10^{-17}$ | | 2000 | | | |

limit of the reaction, is highly underpopulated in comparison to single-channel reactions, because nonequilibrium effects deplete the populations below and above the threshold energy of the lower channel to a stronger extent than those in the case of strong collisions. The low-pressure rate coefficient for the upper channel, thus, is predicted to be much smaller than that expected for a situation in which the lower channel would be absent. Practical examples could not be analyzed realistically at the time of publication of part 1, since neither sufficiently accurate experiments nor sufficiently detailed information on the relevant molecular data were available. The situation now has changed, and in selected cases, one can proceed toward a more quantitative analysis. Previous evaluations of experimental two-channel rate coefficients often neglected the strong coupling between the two channels and, therefore, appear unsatisfactory; see below. The present article tries to overcome these shortcomings. We chose the thermal dissociation of formaldehyde as a particularly well-characterized example for which interesting new insight into the dynamics is just becoming available.

For a long while, the rate coefficients for the thermal decomposition of formaldehyde and the nature of its products were uncertain.[8] The situation today has improved considerably, see the review in ref 9, and results from about the last 25 years now appear to converge[10−22] such that a detailed analysis can be made. At the same time, the photodissociation dynamics has been studied in great detail[23−30] and photolysis quantum yields have been measured.[31−38] It has also become clear[26,29,36,37,39] that the system is not a two- but a three-channel system, with the "normal" molecular-elimination channel

$$H_2CO \rightarrow H_2 + CO \qquad (1)$$

having the lowest reaction threshold, the radical-forming channel

$$H_2CO \rightarrow H + HCO \qquad (2)$$

proceeding as a simple bond fission with a higher threshold energy and an additional, "unusual", intramolecular-hydrogen-abstraction channel producing molecular fragments, although it follows the radical pathway in its initial stage.[26,29,39]

$$H_2CO \rightarrow H\cdots HCO \rightarrow H_2 + CO \qquad (3)$$

Detailed ab initio calculations of the potential energy surface of the electronic ground state of $H_2CO$ have been extended into the dissociation range,[40−44] and precise spectroscopic and thermochemical parameters of relevance for the thermal dissociation[27] are also available now. One should even think about a fourth channel involving electronically excited triplet formaldehyde $H_2CO(S_0) \rightarrow H_2CO(T_1) \rightarrow H + HCO$ which has been demonstrated to contribute to formaldehyde photodissociation.[24,28,42] However, the threshold energy of this channel is too high for a contribution to the thermal dissociation.

On the basis of the given pieces of information today one can approach a more realistic modeling of the thermal dissociation rates of formaldehyde than was possible previously. This is the goal of the present article. One may use this approach for an extrapolation of the experimental results into wider and not easily accessible ranges of conditions. Earlier modeling, for example of tunneling contributions of the molecular channel (1) to the thermal dissociation rates,[45] of specific rate constants[46,47] $k_i(E,J)$ for the molecular channel (1) and the radical channel (2), of isotope effects,[45,46] and of falloff curves[7,19,45] are helpful for this task, but they need to be adapted to the improved database available today. An important aspect of the analysis is the relation between thermal and photochemical activation experiments, such as elaborated in detail in the present work. The following article first focuses attention on the thermal dissociation in the low-pressure range (neglecting tunneling). The question[25,44] of the threshold energy of channel 1 is investigated again, and a new value is fitted from the thermal branching ratio. The article only briefly considers the transition to the high-pressure limit which has not been accessed experimentally as of yet. Earlier modeling of the reaction in the transition range to the high-pressure limit such as presented in refs 7, 19, and 45 have to be revised in view of the three-channel character of the reaction which now looks well established.

## II. Experimental Database

The prediction of thermal dissociation rate coefficients in the low-pressure range cannot yet be made without fitting the modeling to experimental data at some point. In particular, energy transfer data are not well-known in advance. Therefore, a review of the kinetic database will be the starting point of our analysis.

Table 1 and Figure 1 summarize experimental results for $k_{0,Mol}$ and $k_{0,Rad}$ together with experimental details of relevance for the analysis. $k_{0,Mol}$ and $k_{0,Rad}$ denote the pseudo-first-order rate coefficients for dissociation into molecular and radical products, respectively. To arrive at a better comparison of the experimental

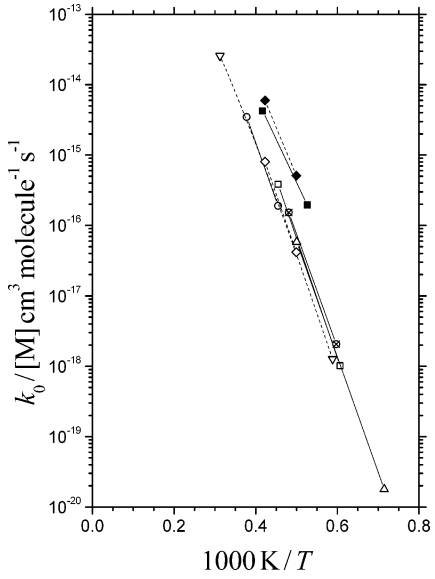


**Figure 1.** Pseudo-second-order rate coefficients $k_0$ of the thermal decomposition of formaldehyde in the low-pressure range; experimental results for M = Ar (full lines) and M = Kr (dashed lines) with the formation of molecular products ($k_{0,Mol}$, filled symbols) and of radical products ($k_{0,Rad}$, open symbols), measurements from ref 13 (○), ref 14 (□), ref 15 (▽), ref 16 (△),ref 17 (◇), and ref 19 (⊗); see Table 1. The symbols denote the limits of the experimental ranges.

data, rate coefficients for $T = 2000$ K are also shown in Table 1. Averaging of the best values for $k_{0,Rad}$ at 2000 K gives[13,14,16,19] $k_{2,Rad}/[Ar] = 5.8 \times 10^{-17}$ cm$^3$ molecule$^{-1}$ s$^{-1}$ and[15,17] $k_{0,Rad}/[Kr] = 3.9 \times 10^{-17}$ cm$^3$ molecule$^{-1}$ s$^{-1}$. The values of $k_{0,Mol}/[Ar] = 4.1 \times 10^{-16}$ cm$^3$ molecule$^{-1}$ s$^{-1}$ from ref 14 and $k_{0,Mol}/[Kr] = 5.0 \times 10^{-16}$ cm$^3$ molecule$^{-1}$ s$^{-1}$ from ref 17 are clearly about a factor of 10 larger than the corresponding values of $k_{0,Rad}/[M]$. The apparent activation energies for the molecular channel appear to be somewhat smaller than those for the radical channel. Over the indicated pressure range of 0.2−3 bar no deviations from second-order kinetics were observed. An extension up to 20 bar[20] also did not yet show a change of reaction order within the experimental accuracy. The data from Table 1 constitute the reference base for our modeling such as elaborated in the following. We consider the experiments from ref 17 in the bath-gas Kr as the most precise and use them for fitting $E_0(1)$ and $\langle\Delta E(Kr)\rangle$. $\langle\Delta E(Ar)\rangle$ is fitted on the basis of the averaged $k_{0,Rad}$ (2000 K).

## III. Master Equation for Multi-channel Reactions

The 2D, rovibrational master equation underlying our modeling in continuous form is written as[7]

$$d[A(E,J)]/dt \approx -\left\{Z[M] + \sum_i k_i(E,J)\right\}[A(E,J)] + Z[M] \sum_{J'=0}^{\infty} \int_0^{\infty} P(E,J/E',J')[A(E',J')]\, dE' \quad (4)$$

with the collision frequency $Z$ for energy transfer, the specific rate constants $k_i(E,J)$ for dissociation in the channels $i$, and the rovibrational transition probabilities $P(E,J/E',J')$ for collisional energy transfer from state $(E',J')$ to state $(E,J)$. The master equation can sometimes be solved analytically in steady state even for two dimensions such as demonstrated in ref 2. Because of our limited knowledge on the rotational contribution to energy transfer, however, we neglect the rotational part of the problem and replace eq 4 by a set of decoupled 1D master equations

$$d[A(E,J)]/dt \approx -\left\{Z[M] + \sum_i k_i(E,J)\right\}[A(E,J)] + Z[M] \int_0^{\infty} P(E/E')A(E',J')\, dE' \quad (5)$$

which are combined only at the level of the final calculation of the rate coefficient. For strong collisions, the solution of the master equation is given by the usual, "trivial", expressions from unimolecular rate theory adapted to the multichannel situation considered here; see part 1.[7] For weak collisions, however, the solution involves a more subtle approach such as elaborated in part 1[7] on the basis of the results from ref 2. In the following, we focus attention on the low-pressure limit which is relevant for the experiments summarized in section II. Before doing that, we have to characterize the specific rate constants $k_i(E,J)$ governing the multichannel branching of the reaction at a given $E$ and $J$.

## IV. Modeling of Specific Branching Ratios $V_i(E,J)$

The molecular channel (1) is almost thermoneutral but proceeds over an activation barrier which is of the order of $E_{0,1} = 342.7$ (±1.3) kJ mol$^{-1}$, that is, $E_{0,1}/hc = 28645$ cm$^{-1}$, such as obtained from advanced ab initio calculations.[44] This value contrasts with the value of $E_{0,1} = 331.4$ (±3.3) kJ mol$^{-1}$, that is, $E_{0,1}/hc = 27700$ cm$^{-1}$, which was obtained[25] by a fit of Rice−Ramsperger−Kassel−Marcus (RRKM) rates to experimental rates using experimental densities of states; see the discussion given below. However, because of the dispute about the value of $E_{0,1}$, we performed our analysis for both values and we finally also tried to derive a value from the thermal dissociation experiments. Our result ($E_{0,1} = 339.7$ (±3.6) kJ mol$^{-1}$, i.e., $E_{0,1}/hc = 28400$ cm$^{-1}$) essentially agrees with the ab initio result; see below.

It is obvious that, because of tunneling through the activation barrier, the true low-pressure limiting range of the reaction cannot be reached experimentally. However, neither the experiments nor the simplified modeling of the pressure dependence from refs 19 and 45 show noticeable deviations from an apparent second-order behavior for the conditions of the experiments summarized in Table 1. In addition, the conditions of the experiments from Table 1 in ref 45 were all shown to correspond closely to the low-pressure limit derived in the absence of tunneling. We, therefore, in the following consider low-pressure unimolecular reaction behavior in the absence of tunneling only.

Once molecules have reached energies above the threshold energy of the radical channel[27] $E_{0,2} = 362.8$ (±0.006) kJ mol$^{-1}$, that is, $E_{0,2}/hc = 30328.5$ cm$^{-1}$, there is branching into radical (channel 2) and molecular fragments (channels 1 and 3). This branching is characterized by the specific rate constants $k_i(E,J)$ with $i = 1-3$ for the three channels (1−3). Modeling of $k_1(E,J)$ by standard, rigid-activated, complex RRKM theory including tunneling, and of "$k_2(E,J)$" by simplified statistical adiabatic channel method (SACM) calculations, in ref 46 showed substantial differences between the two channels. (In the following, "$k_2(E,J)$" from the SACM calculations of ref 46 is understood to correspond to the sum of $k_2(E,J)$ and $k_3(E,J)$.) Once the radical channel is open energetically, "$k_2(E,J)$" with increasing energy quickly and markedly exceeds $k_1(E,J)$. In addition, rotational channel switching in ref 46 was shown to occur such that channels 2 and 3, for $J$ above some switching value $J_{SW}$, become energetically more favorable than the

molecular channel (1). "$k_2(E,J)$" increases much faster with increasing energy to much larger values than $k_1(E,J)$. For this reason, the semiquantitative results from ref 46 are still largely sufficient to characterize the branching between channels 1 and 2 + 3 as a function of $E$ and $J$, provided that the correct threshold energies $E_{0,i}$ are known. It is, therefore, essential that the $E_{0,i}(J)$ values, which lead to rotational channel switching, are updated, and the $k_i(E,J)$ values from ref 46 are shifted along the energy axis accordingly.

Rotational channel switching occurs when the difference between the threshold energies of channels 1 and 2 as a function of $J$, that is, $\Delta E_0(J) = E_{0,2}(J) - E_{0,1}(J)$, is equal to zero. The rigid transition state of channel 1 is approximately characterized by

$$E_{0,1}(J) \approx E_{0,1}(J{=}0) + B^{\ddagger}\mathrm{hc}J(J+1) \qquad (6)$$

where $B^{\ddagger}$ has been calculated[40] ab initio to be equal to $B^{\ddagger} = 1.12\ \mathrm{cm}^{-1}$. The centrifugal barriers for the radical-forming bond-fission channel (2) on the other hand can be derived with the ab initio potential from ref 43; see appendix. This, for example, leads to

$$E_{0,2}(J) \approx E_{0,2}(J{=}0) + C_{\nu}[J(J+1)]^{\nu} \qquad (7)$$

with $\nu \approx 1.2$ (over the range $J = 0-50$), and $C_{\nu}/\mathrm{hc} \approx 0.0115\ \mathrm{cm}^{-1}$. Employing the experimental value $E_{0,2}(J{=}0)/\mathrm{hc} = 30328.5\ \mathrm{cm}^{-1}$ from ref 27 and either $E_{0,1}(J{=}0)/\mathrm{hc} \approx 27700\ \mathrm{cm}^{-1}$ from the analysis[25] of experimental $k_1(E)$, our fitted $E_{0,1}(J{=}0)/\mathrm{hc} \approx 28400\ \mathrm{cm}^{-1}$ or $E_{0,1}(J{=}0)/\mathrm{hc} \approx 28645\ \mathrm{cm}^{-1}$ from the ab initio calculations,[44] one derives $J_{SW} \approx 49$, $\approx 42$, or $\approx 39$, respectively. There has been considerable discussion[25,44] about the value of the barrier height $E_{0,1}(J{=}0)$ and the measured specific rate constants $k_1(E,J)$ in relation to RRKM-type modeling. The controversy is directly related to discrepancies (by about a factor of 6) between measured and calculated anharmonic vibrational densities of states.[25] While this discrepancy has not been resolved so far, it was noted in ref 44 that RRKM-type calculations (like those performed in refs 46 and 47) come into agreement with measured $k_1(E,J)$ values when the higher ab initio value of $E_{0,1}(J{=}0)$ is used together with calculated anharmonic densities of states. Our analysis of thermal branching ratios supports the higher value of $E_{0,1}$. Nevertheless, the reasons for measuring[25] a factor of 6 higher densities of states than expected remain unclear.

Equation 7 serves for quick characterizations of rotational channel switching. For a more precise analysis, the values of $E_{0,2}(J)$ are calculated in detail and in the present work are used instead of eq 7. Figure 2 represents the results for $E_{0,2}(J)$ for $E_{0,1}(J)$ on the basis of $E_{0,1}(J{=}0)/\mathrm{hc} = 28\,645\ \mathrm{cm}^{-1}$.

For analyzing thermal rate coefficients in the low-pressure limit, not absolute values of $k_i(E,J)$ but branching ratios are of interest. We define these specific branching ratios by

$$V_i(E,J) = k_i(E,J) / \sum_i k_i(E,J) \qquad (8)$$

Expressing $k_i(E,J)$ in terms of statistical unimolecular rate theory by $W_i(E,J)/\mathrm{h}\rho(E,J)$, the controversial $\rho(E,J)$ cancels and the $V_i(E,J)$ values are given by

$$V_i(E,J) = W_i(E,J) / \sum_i W_i(E,J) \qquad (9)$$

where $W_i(E,J)$ denote the number of open channels (or cumulative reaction probabilities). These quantities are taken from ref 46 and employed for deriving $V_1(E,J)$. Following the format used in ref 7, for $J < J_{SW}$ one obtains

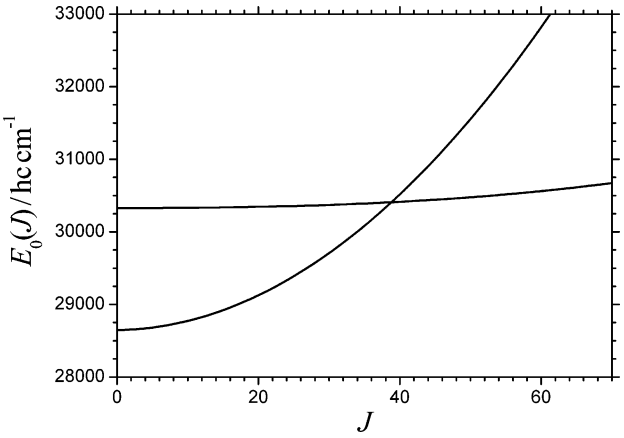


**Figure 2.** Centrifugal barriers for channel 1, $E_{0,1}(J)$, and for channels 2 and 3, $E_{0,2}(J)$ (calculations with $E_{0,1}(J{=}0)/\mathrm{hc} = 28\,645\ \mathrm{cm}^{-1}$ and $E_{0,2}(J{=}0)/\mathrm{hc} = 30328.5\ \mathrm{cm}^{-1}$, see text).

for $E < E_{0,2}(J)$

$$V_1(E,J) = 1$$

for $E > E_{0,2}(J)$

$$V_1(E,J) \approx 0.05\ (\pm 0.02) + 0.95\ (\pm 0.02)\ \exp\{-[E - E_{0,2}(J)]/\delta\} \qquad (10)$$

with $\delta/\mathrm{hc} = 100\ (\pm 50)\ \mathrm{cm}^{-1}$. The indicated variations of the parameters include the variations found for the range $0 < J < J_{SW}$, where $J_{SW}$ corresponds to that value of $J$ where rotational channel switching occurs. For $J > J_{SW}$, $V_1(E,J)$ quickly becomes negligibly small.

While

for $E < E_{0,2}(J{=}0)$

$$V_2(E,J) = V_3(E,J) = 0 \qquad (11)$$

is trivially fulfilled, the specification of $V_2(E,J)$ and $V_3(E,J)$ at $E > E_{0,2}(J)$ is still relatively uncertain. Only recently channel 3 has been modeled by classical trajectory calculations[39] on the global ab initio potential from ref 43. Channel 3 seems to open up at $E = E_{0,2}$. The presence of channel 3 provides an explanation for the appearance of molecular fragments in photolysis experiments[32-34] employing excitation energies larger than those of $E_{0,2}$ ($\lambda \leq 330$ nm). Although the fine details of $k_2(E,J)$ and $k_3(E,J)$ are still not known accurately, both the classical trajectory calculations from ref 39 and the quantum yield measurements over the range 330−310 nm from refs 32−34 at least allow for a rough characterization of the branching ratio $k_2(E)/[k_2(E) + k_3(E)]$. From the trajectory calculations (see Figure 5 of ref 39), one reads

$$V_2(E,J{=}0) = k_2(E,J{=}0)/[k_2(E,J{=}0) + k_3(E,J{=}0)] \approx \exp[-(E - E_{0,2}(J{=}0))/\mathrm{hc}1200\ \mathrm{cm}^{-1}] \qquad (12)$$

There was some evidence in ref 39 that eq 6 does not change much with the total $J$.

The second access to $V_2(E,J)$ via photolysis quantum yields $\phi(\lambda)$ seems to lead to different results. The differences, however,

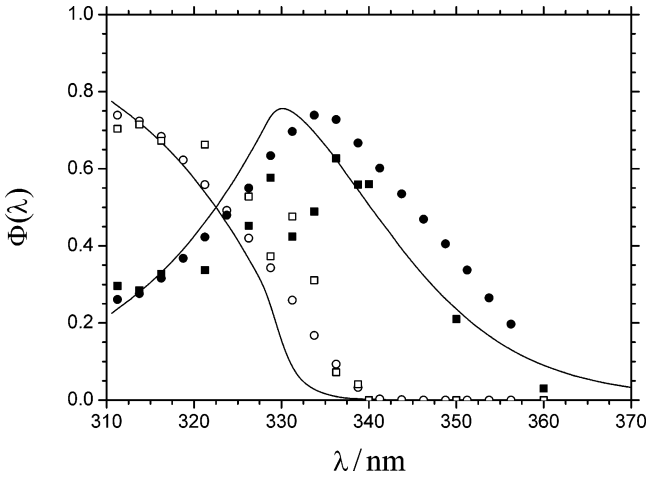


**Figure 3.** Quantum yields $\phi_{Mol}(\lambda)$ and $\phi_{Rad}(\lambda)$ of molecular and radical fragments in formaldehyde photolysis (at 298 K and 1 bar of $N_2$) (□ and ○, evaluated experimental data for $\phi_{Rad}(\lambda)$ from refs 37 and 38, respectively; ■ and ●, the same for $\phi_{Mol}(\lambda)$; full lines, preliminary modeling from ref 48 corresponding to eqs 13−15, see text).

may be explained by rotational effects in the thermal photolysis experiments. A brief summary of the analysis[48] of $\phi(\lambda)$ from ref 38 is given in the following. One may assume that photolysis at $\lambda > 310$ nm after electronic excitation of $H_2CO$ is characterized by internal conversion such that the production of molecular and radical products is governed by the competition between channels 1−3 in the electronic ground state. $\phi(\lambda)$ then corresponds to the thermal average over $V_1(E,J) + V_3(E,J)$ for molecular products and over $V_2(E,J)$ for radical products. There are two ranges to be considered: At $\lambda < 330$ nm, $\phi(\lambda)$ was found to be pressure independent; at $\lambda > 330$ nm, pressure-dependent $\phi(\lambda)$ was observed. The pressure independence at $\lambda < 330$ nm is easily explained by the large values of "$k_2(E,J)$" modeled in ref 46. The pressure dependence at $\lambda > 330$ nm is a consequence of the much smaller values of $k_1(E,J)$, in particular, in the tunneling range of reaction 1 which becomes of importance in the photolysis. The two ranges require different representations. The analysis of the measured $\phi_i$ ($\lambda$, 298 K, 1 bar) in ref 48 was done by thermal averaging over $\phi_i(E,J)$ where $E = h\nu + E_{rot}(T)$. (The subscript $i$ denotes molecular and radical products, respectively; $E_{rot}(T)$ is the rotational energy; $H_2CO$ is represented as a symmetric top; see appendix. Vibrational excitation remains negligible at 298 K.) For experimental pressures of 1 bar such as documented in refs 31−38, at $J \le J_{SW}$ and $E \le E_{0,2}(J) + \delta$, $\phi_{Mol}(E,J)$ for simplicity are represented by an exponential expression of the type

$$\phi_{Mol}(E,J) \approx \{1 + c_1 \exp[-(E - E_{0,1}(J))/\epsilon_1]\}^{-1} \quad (13)$$

while $\phi_{Rad}(E,J) \approx 0$ ($\delta$ is defined in eq 10). At $E \ge E_{0,2}(J) + \delta$ and all $J$, an exponential expression of the type

$$\phi_{Mol}(E,J) \approx (1 - c_2) \exp[-(E - E_{0,2}(J) - \delta)/\epsilon_2] \quad (14)$$

is tentatively applied by analogy to eq 12, while

$$\phi_{Rad}(E,J) \approx c_2 + (1 - c_2)\{1 - \exp[-(E - E_{0,2}(J) - \delta)/\epsilon_2]\} \quad (15)$$

The parameters $c_1$ and $\epsilon_1$ govern $\phi_i(\lambda)$ in the tunneling range (at $E < E_{0,1}(J)$ and $J < J_{SW}$) and can be fitted nearly independent of the parameters $c_2$ and $\epsilon_2$ governing $\phi_i(\lambda)$ in the range 310−330 nm. Figure 3 compares measured and fitted quantum yields (from ref 48). The lower value of $E_{0,1}/hc$ (= 27 700 $cm^{-1}$) always gives too large values of $\phi_{Mol}$ near its maximum experimental value of 0.63[37]−0.74.[38] The same would occur, if the result of eq 12 (i.e., eqs 14 and 15 with $c_2 = 0$ and $\epsilon_2/hc = 1200$ $cm^{-1}$) from the trajectory calculations would apply. Fitting the parameters $c_1$, $\epsilon_1$, $c_2$, and $\epsilon_2$ to the averaged experimental results for $\phi(\lambda)$ given in ref 38, instead, give the following parameters, $c_1 = 3$, $\epsilon_1/hc = 700$ $cm^{-1}$, $c_2 = 0.16$, $\epsilon_2/hc = 1500$ $cm^{-1}$. The corresponding fits are included in Figure 3. Equations 14 and 15, with $V_2(E,J) \approx \phi_{Rad}(E,J)$ and $V_3(E,J) \approx \phi_{Mol}(E,J)$ and the fitted parameters $c_2$ and $\epsilon_2$, therefore, are used for the range $E \ge E_{0,2}(J) + \delta$. It should be emphasized that eqs 13−15 so far are only tentative. Equation 13 is related to the energy dependence of $k_1(E,J)$ in the tunneling range, and eqs 14 and 15 follow the exponential form of the trajectory calculations[39] but require modifications which are possibly due to rotational effects. Nevertheless, the fact that the experimental $\phi(\lambda)$ is reproduced within uncertainty supports our fit. However, the fit is not unique, and it was optimized in our work by comparison with the thermal branching ratio $k_{0,Mol}(M=Kr)/k_{0,Rad}(M=Kr)$; see below. The apparent discrepancy between eqs 12 and 15 may be attributed to the fact that photolysis experiments cover wide rotational distributions while eq 12 was derived for $J = 0$.

## V. Modeled Total Low-Pressure Rate Coefficients

The total rate coefficients in the low-pressure limit of the thermal decomposition $k_0$, being the sum of the radical and molecular contributions $k_{0,Rad}$ and $k_{0,Mol}$, respectively, can be determined without knowing the specific branching ratios $V_i(E,J)$ elaborated in section IV. Solving the master eq 5 for $[M] \rightarrow 0$ in the way described in refs 2, 7, 49, and 50 leads to

$$k_0/[M] \approx \beta_c Z_{LJ}[\rho_{vib,h}(E_0)kT/Q_{vib}] \exp(-E_0/kT) F_E F_{anh} F_{rot} \quad (16)$$

with the various factors defined in ref 50 and characterized more explicitly in the appendix. The collision efficiency $\beta_c$ is related to the average energy $\langle\Delta E\rangle$ transferred per collision by[2] $\beta_c/(1 - \beta_c^{1/2}) \approx -\langle\Delta E\rangle/F_E kT$. In a multichannel reaction in the low-pressure region, $k_0$ is equal to the sum of the individual channel rate constants, that is, $k_0 = k_{0,1} + k_{0,2} + k_{0,3} = k_{0,Mol} + k_{0,Rad}$ in the present case. By fitting the experimental value of $k_{0,Mol} + k_{0,Rad}$ at 2000 K, $\langle\Delta E\rangle$ is fixed and afterward kept constant independent of temperature such as this has been approximately observed in the experimental examples analyzed with eq 16; see, for example, refs 50−52.

The only difference between single- and multichannel systems is in the rotational factor $F_{rot}$ which in the latter case has to account for rotational channel switching.[1] Following the method of ref 50, we determined the effective ratio $I^+/I$ of moments of inertia from the detailed determination of $E_0(J)$ accounting for rotational channel switching. Combining this with the maximum rotational factor, $F_{rot,max}$, in the absence of centrifugal barriers leads to the rotational factors $F_{rot}$ such as given in the appendix. Fitting eq 16 to the experimental value of $k_0$ at 2000 K, that is, $k_0/[Kr] \approx 5.4 \times 10^{-16}$ $cm^3$ $molecule^{-1}$ $s^{-1}$ (see section II), for given dissociation energies $E_{0,1}$ and $E_{0,2}$ leads to a value for $\langle\Delta E\rangle$. As $E_{0,2}$ has been determined experimentally with high precision, one may ask for the influence of the chosen $E_{0,1}$ on the fitted $\langle\Delta E\rangle$. Evaluating eq 16 with $E_{0,1}/hc = 27\,700$ $cm^{-1}$ leads to $-\langle\Delta E\rangle/hc \approx 250$ ($\pm 50$) $cm^{-1}$ in agreement with the analysis from ref 19 which also used eq 16. Using the higher

value $E_{0,2}/hc = 28\,645\ cm^{-1}$ on the other hand leads to $-\langle\Delta E\rangle/hc = 50\ cm^{-1}$ for M = Kr. This value is smaller than the values measured for larger excited molecules for which $-\langle\Delta E\rangle/hc = 180-250\ cm^{-1}$ was determined[3-6] at $E/hc = 30\,000\ cm^{-1}$. However, it is in line with experimental values for smaller molecules such as $HO_2$ ($-\langle\Delta E\rangle/hc = 20\ cm^{-1}$ for M = Ar at $E_0/hc = 17\,000\ cm^{-1}$) and $CH_4$ ($-\langle\Delta E\rangle/hc = 50\ cm^{-1}$ for M = Ar at $E_0/hc = 36\,100\ cm^{-1}$); see refs 51 and 52, respectively. Close agreement with the $\langle\Delta E\rangle$ values for these small molecules is obtained keeping in mind that $\langle\Delta E\rangle$ is approximately proportional to the energy.[3-6] Like the photolysis quantum yields, also the low-pressure rate coefficients appear to be consistent only with the larger values of $E_{0,1}$. In our final analysis, $E_{0,1}/hc = 28400\ cm^{-1}$ was fitted from the thermal-branching ratios; see below. $k_0/[Kr] = 5.4 \times 10^{-16}$ cm$^3$ molecule$^{-1}$ s$^{-1}$ at 2000 K from ref 17 then leads to $-\langle\Delta E\rangle/hc = 54\ cm^{-1}$ for M = Kr. On the basis of analysis of the experiments in Ar on the average $k_{0,Rad}$ at 2000 K only, and not on the less certain $k_{0,Mol}$ from ref 14, $-\langle\Delta E\rangle/hc = 64\ cm^{-1}$ is obtained for M = Ar. At the same time, one obtains

$$(k_{0,Mol} + k_{0,Rad})/[Ar] \approx 1.2 \times 10^{-8} \exp(-33\,410\ K/T)\ cm^3\ molecule^{-1}\ s^{-1} \quad (17)$$

over the temperature range 1400−3200 K (with $(k_{0,Mol} + k_{0,Rad})/[Ar] = 6.6 \times 10^{-16}$ cm$^3$ molecule$^{-1}$ s$^{-1}$ at 2000 K). For M = Kr

$$(k_{0,Mol} + k_{0,Rad})/[Kr] = 9.7 \times 10^{-9} \exp(-33\,410\ K/T)\ cm^3\ molecule^{-1}\ s^{-1} \quad (18)$$

is obtained over the range 1400−3200 K on the basis of $(k_{0,Mol} + k_{0,Rad})/[Kr] = 5.4 \times 10^{-16}$ cm$^3$ molecule$^{-1}$ s$^{-1}$ at $T = 2000$ K. The modeled eqs 17 and 18 probably provide more accurate temperature coefficients than those of the experimental values from Table 1. Nevertheless, the observed small differences of the temperature coefficients are well within the experimental uncertainties.

## VI. Low-Pressure Thermal Branching Ratios

In the low-pressure range of the reaction the specific branching ratios $V_i(E,J)$ are convoluted with nonequilibrium populations $g(E,J)$ of states which markedly differ from equilibrium populations. As a consequence, upper channels are suppressed. The treatment from part I[7] in analytical form provides a simple and quantitative description for this effect. The nonequilibrium population factor $h(E) = g(E)/f(E)$ is derived by solving the 1D master equation for an exponential collision model. Below the lowest dissociation energy, $E_{0,min} = \min(E_{0,1},E_{0,2})$, has the form

$$h(E) \approx 1 - [F_E kT/(\alpha + F_E kT)] \exp[-(E_{0,min} - E)/F_E kT] \quad (19)$$

where the average energy $\alpha$ transferred per down collision is related to $\langle\Delta E\rangle$ through[2]

$$\alpha \approx -\langle\Delta E\rangle/2 + (\langle\Delta E\rangle^2/4 - \langle\Delta E\rangle F_E kT)^{1/2} \quad (20)$$

(note that $\langle\Delta E\rangle < 0$). At $E > E_{0,min}$, $h(E)$ has the form

$$h(E) \approx \{Z_{LJ}[M]/[k_1(E) + k_2(E) + k_3(E)]\} \times \{\alpha/(\alpha + F_E kT)\} \exp[-(E - E_{0,min})/\alpha] \quad (21)$$

The total low-pressure rate coefficient with this nonequilibrium population factor, for the sum of channels 1, 2, and 3, then is calculated via

$$k_0 = \int_{E_{0,min}}^{\infty} h(E)f(E)[k_1(E) + k_2(E) + k_3(E)]\ dE \quad (22)$$

which gives

$$k_0/[M] = \beta_c Z_{LJ}[\rho_{vib,h}(E_{0,min})kT/Q_{vib}] \exp(-E_{0,min}/kT)F_E F_{anh} \quad (23)$$

The collision efficiency follows as $\beta_c = [\alpha/(\alpha + F_E kT)]^2$ or $\beta_c/(1 - \beta_c^{1/2}) = -\langle\Delta E\rangle/F_E kT$. The summation over $J$ finally leads to eq 16, that is, by averaging over $J$ the factor $F_{rot}$ arises such as evaluated in section V.

The thermal rate coefficients for individual channels follows analogous to eq 22. For example, one has

$$k_{2,0} = \int_{E_{0,min}}^{\infty} h(E)f(E)k_2(E)\ dE \quad (24)$$

which introduces the specific branching ratio $V_2(E) = k_2(E)/[k_1(E) + k_2(E) + k_3(E)]$ from section IV into the integral. Again, averaging over $J$ is done in the end. For the present situation, the two ranges $J > J_{SW}$ and $J \le J_{SW}$ require different treatments. We first consider the range $J > J_{SW}$. In this case, channel 1 can practically be neglected and channels 2 and 3 have the threshold energy $E_{0,min}(J) = E_{0,2}(J)$. The integral of eq 24 then samples $V_2(E,J)$ from eq 15 with the factor $\exp\{-[E - E_{0,2}(J) - \delta][1/\alpha + 1/F_E kT]\} = \exp\{-[E - E_{0,2}(J) - \delta]/\gamma\}$ where $\gamma = \alpha F_E kT/(\alpha + F_E kT)$ denotes the average energy per up collision (with $\langle\Delta E\rangle = \gamma - \alpha$). The result, for $J \ge J_{SW}$, with eq 15 follows as

$$k_{2,0}(J)/k_0 = 1 - \{1 - V_2[E_{0,2}(J) + \delta]\}\epsilon_2/(\gamma + \epsilon_2) \quad (25)$$

Averaging over $J$ in symmetric top approximation roughly gives

$$k_{2,0}/k_0 \approx c_2 f(J \ge J_{SW}) \quad (26)$$

where $f(J \ge J_{SW})$ is the fraction of the rotational distribution with $J \ge J_{SW}$; see below. The contribution to $k_{2,0}/k_0$ from the range $J < J_{SW}$ is much smaller. In this case, $k_2(E)$ becomes appreciable only at $E > E_{0,2}(J) + \delta$, and the lower limit of the integral of eq 24 now is equal to $E_{0,1}(J)$. The resulting $k_{2,0}/k_0$ (for $J < J_{SW}$ and with eq 10) according to ref 7 can be approximated by

$$k_{2,0}(J)/k_0 \approx c_2 \exp\{-[E_{0,2}(J) + \delta - E_{0,1}(J)]/\gamma\} \quad (27)$$

The final thermal branching ratio $k_{2,0}/k_0$, after rotational averaging and accounting for rotational channel switching, is given by

$$k_{2,0}/k_\infty \approx Q_{rot}^{-1} \sum_{J=0}^{\infty} (2J+1) \sum_{K=-J}^{+J} \times [k_{2,0}(J)/k_0] \exp[-E_{rot}(J,K)/kT] \quad (28)$$

with $E_{rot}(J,K) = BJ(J+1) + (A - B)K^2$.

The resulting thermal branching ratios $k_{2,0}/k_0$ are summarized in Table 2 as a function of temperature. The table separately shows the contributions to $k_{2,0}/k_0$ from the ranges of $J < J_{SW}$ and $J \ge J_{SW}$. For a comparison with the simple estimate from eq 26, the table also includes $f(J \ge J_{SW})$. The contribution to $k_{2,0}/k_0$ from the range $J < J_{SW}$ indeed is much smaller than that from $J \ge J_{SW}$, but it cannot be neglected. One also finds that the formation of molecular products via channel 1 is so much

**TABLE 2: Modeled Total Low-Pressure Rate Coefficients $k_0$/[Kr] (in cm$^3$ molecule$^{-1}$ s$^{-1}$) and Thermal Branching Ratios $k_{2,0}/k_0$ for the Radical-Forming Channel 2[a]**

| $T$/K | $k_0$/[Kr] | $k_{2,0}/k_0$ | $(k_{2,0}/k_0)_{\mathrm{low}J}$ | $(k_{2,0}/k_0)_{\mathrm{high}J}$ | $f(J>J_{\mathrm{SW}})$ |
|---|---|---|---|---|---|
| 1400 | $2.4 \times 10^{-19}$ | 0.036 | 0.004 | 0.032 | 0.118 |
| 1700 | $2.5 \times 10^{-17}$ | 0.055 | 0.006 | 0.049 | 0.174 |
| 2000 | $5.4 \times 10^{-16}$ | 0.074 | 0.007 | 0.067 | 0.229 |
| 2500 | $1.4 \times 10^{-14}$ | 0.106 | 0.009 | 0.096 | 0.311 |
| 3200 | $1.6 \times 10^{-13}$ | 0.147 | 0.011 | 0.136 | 0.408 |

[a] "Low $J$", $J < J_{\mathrm{SW}}$; "high $J$", $J \geq J_{\mathrm{SW}}$; $f(J > J_{\mathrm{SW}})$, equilibrium population of states with $J \geq J_{\mathrm{SW}}$; see text.

**TABLE 3: Thermal Branching Ratios at $T = 2000$ K[a]**

| $E_{0,1}$[b]/hc cm$^{-1}$ | $k_{2,0}/k_0$ | $(k_{2,0}/k_0)_{\mathrm{low}J}$ | $(k_{2,0}/k_0)_{\mathrm{high}J}$ |
|---|---|---|---|
| 27700 | 0.042 | 0.004 | 0.038 |
| 28000 | 0.054 | 0.005 | 0.049 |
| 28300 | 0.069 | 0.007 | 0.062 |
| 28400 | 0.074 | 0.007 | 0.067 |
| 28647 | 0.091 | 0.008 | 0.083 |

[a] See Table 2. [b] Dependence on the threshold energy $E_{0,1}$ of channel 1, see text.

less important in comparison to that from channel 3 that tunnelling corrections will be negligible.

Calculations of the thermal branching ratios also show the sensitivity of $k_{2,0}/k_0$ on the value of $E_{0,1}$. Table 3 shows modeled values of $k_{2,0}/k_0$ at 2000 K as a function of the value of $E_{0,1}$. One realizes that the preferred experimental value for M = Kr from ref 17 is best fitted with $E_{0,1}/\mathrm{hc} = 28\,400$ cm$^{-1}$. The ab initio value of $E_{0,1}/\mathrm{hc} = 28\,645$ cm$^{-1}$ from ref 44 is within the estimated uncertainty of $\pm 300$ cm$^{-1}$ of the present modeling and the experiments. Since the experimental $k_0$ value for M = Ar does not appear to be reliable enough, we use the experimental averaged $k_{2,0}$ value for M = Ar at 2000 K and the modeled branching ratio for an improved specification of $k_0$. Likewise, the temperature dependencies of $k_{2,0}$ and $k_0$ are taken from the modeling. The following results are finally obtained over the range 1400−3200 K (in cm$^3$ molecule$^{-1}$ s$^{-1}$)

$$k_{0,\mathrm{Mol}}/[\mathrm{Ar}] = 9.4 \times 10^{-9} \exp(-33\,140\ \mathrm{K}/T) \quad (29)$$

$$k_{0,\mathrm{Rad}}/[\mathrm{Ar}] = 6.2 \times 10^{-9} \exp(-36\,980\ \mathrm{K}/T) \quad (30)$$

$$k_{0,\mathrm{Mol}}/[\mathrm{Kr}] = 7.7 \times 10^{-9} \exp(-33\,110\ \mathrm{K}/T) \quad (31)$$

$$k_{0,\mathrm{Rad}}/[\mathrm{Kr}] = 4.1 \times 10^{-9} \exp(-36\,910\ \mathrm{K}/T) \quad (32)$$

They are compared in Figure 4 with the experimental results. Within uncertainty, good agreement is obtained. The present modeling extends the temperature ranges, in particular for $k_{0,\mathrm{Mol}}$ which is more difficult to measure.

## VII. Modeled High-Pressure Rate Coefficients

In the high-pressure limiting range of the reaction, equilibrium populations of excited molecular states are established such that the thermal dissociation rate constants for the individual channels are easily formulated as

$$k_{\infty,i} = \sum_{J=0}^{\infty} (2J+1) \int_{E_{0,i}(J)}^{\infty} k_i(E,J) f(E,J) \mathrm{d}E \quad (33)$$

No experimental data for rate coefficients in the high-pressure limit or in the intermediate falloff are available as of yet. Nevertheless, as falloff curves and high-pressure rate coefficients have been modeled before,[19,45] it appears of interest to revise these previous estimates on the basis of present knowledge.

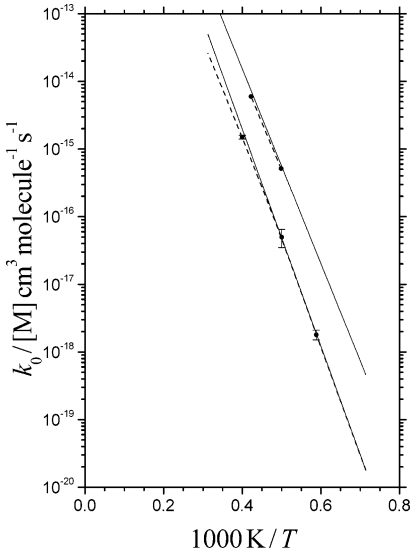


**Figure 4.** Comparison of low-pressure rate coefficients for the formation of molecular products ($k_{0,\mathrm{Mol}}$) and of radical products ($k_{0,\mathrm{Rad}}$) from experiments (dashed lines, from Table 1) with modeling results (full lines, from eqs 29−32 of this work. (The outer filled circles limit the range where more than one experiment is available; see Table 1. Data for $k_{0,\mathrm{Rad}}$ with M = Ar and Kr are combined; the error bars represent the scatter of the experimental results. Data for $k_{0,\mathrm{Mol}}$ are taken from ref 17 and eq 31 with M = Kr only.)

The high-pressure rate constant $k_{\infty,1}$ for channel 1 can be estimated by the simple expression from transition state theory

$$k_{\infty,1} = \frac{kT}{h} \frac{Q^{\ddagger}}{Q} \exp(-E_{0,1}/kT) \quad (34)$$

with the rovibrational, rigid-activated complex partition function $Q^{\ddagger}$ based on the ab initio results from refs 41 and 43; see appendix. With the new value of $E_{0,1}$ this leads to

$$k_{\infty,1} \approx 3.4 \times 10^{14} \exp(-44\,050\ \mathrm{K}/T)\ \mathrm{s}^{-1} \quad (35)$$

Tunneling contributions do not play a role over the temperature range 1400−3200 K considered here.[45]

It appears premature to do a detailed calculation of $k_{\infty,2}$ and $k_{\infty,3}$ as long as there are disagreements about the specific branching ratios $V_2(E,J)$ and $V_3(E,J)$; see above. For this reason, we only provide a quick and rough estimate by assuming that $(k_{\infty,2} + k_{\infty,3})/K_{\mathrm{eq}}$ has the standard value of about $3 \times 10^{-10}$ cm$^3$ molecule$^{-1}$ s$^{-1}$ like other addition reactions of H atoms to hydrocarbon radicals ($K_{\mathrm{eq}}$ corresponds to {[H][HCO]/[H$_2$-CO]}$_{\mathrm{eq}}$). Using $K_{\mathrm{eq}}$ from ref 53 (corrected for the new $E_{0,2}$), this leads to $k_{\infty,2} + k_{\infty,3} \approx 7.7 \times 10^{15} \exp(-43\,700\ \mathrm{K}/T)\ \mathrm{s}^{-1}$. Evaluating the results from ref 46, we derive

$$W_2(E,J{=}30) + W_3(E,J{=}30) \propto [E - E_{0,2}(J)]^{1.46} \quad (36)$$

Using $V_2(E,J) = W_2(E,J)/[W_2(E,J) + W_3(E,J)]$ from eq 15 and convoluting $W_2(E)$, $W_3(E)$, and $W_2(E) + W_3(E)$ with the Boltzmann factor and the specific branching ratio from eq 15 then lead to a thermal branching ratio in the high-pressure limit given by

$$k_{\infty,2}/(k_{\infty,2} + k_{\infty,3}) \approx 1 - (1 - c_2)[\epsilon_2/(\epsilon_2 + kT)]^{2.46} \quad (37)$$

Combined with $k_{\infty,2} + k_{\infty,3}$ such as estimated above, this gives a final estimate of

$$k_{\infty,\mathrm{Rad}} \approx 8.0 \times 10^{15} \exp(-44\,150\ \mathrm{K}/T)\ \mathrm{s}^{-1} \qquad (38)$$

and

$$k_{\infty,\mathrm{Mol}} \approx 3.7 \times 10^{13} \exp(-36\,220\ \mathrm{K}/T)\ \mathrm{s}^{-1} \qquad (39)$$

Equations 8 and 39 correspond to $k_{\infty,\mathrm{Rad}}$ (2000 K) $\approx 2 \times 10^6$ $\mathrm{s}^{-1}$ whereas $k_{\infty,\mathrm{Mol}}$ (2000 K) $\approx 5 \times 10^5$ $\mathrm{s}^{-1}$. The present calculations, therefore, confirm the crossover from $k_{\mathrm{Rad}} < k_{\mathrm{Mol}}$ at low pressures to $k_{\mathrm{Rad}} > k_{\mathrm{Mol}}$ at high pressures which was also predicted in refs 19 and 45. However, the difference between $k_{\infty,\mathrm{Rad}}$ (2000 K) and $k_{\infty,\mathrm{Mol}}$ (2000 K) is estimated to be much smaller than that predicted in refs 19 and 45. This change shifts the crossover to pressures above 1000 bar. It is, therefore, hardly of any practical relevance. As falloff calculations from refs 19 and 45 place the center of the falloff curves at pressures of the order of 100 bar, we do not further inspect the falloff curves before more details about the branching between channels 2 and 3 and the corresponding $k_i(E,J)$ values are known.

## VIII. Conclusions

The thermal dissociation of formaldehyde on the three channels (1−3) identified so far is controlled by an interesting superposition of kinetic effects, that is, by collisional channel coupling, rotational channel switching, and channel branching above the threshold for radical formation. Collisional channel coupling requires the solution of master equations which was done analytically in part 1[7] and is used in the present analysis. Rotational channel switching can be treated with the help of the ab initio calculations of the potential from refs 43 and 44. Channel branching can only be quantified by information from formaldehyde photolysis quantum yields[31−38,48] at $\lambda < 330$ nm,-that is, at energies above the threshold energy for radical formation and from classical trajectory calculations such as described in ref 39.

Fitting the average total energy $\langle \Delta E \rangle$ transferred per collision by means of the total rate coefficient for dissociation at 2000 K and fine-tuning the threshold energy $E_{0,1}(J=0)$ of channel 1 by means of the thermal branching ratio $k_{0,\mathrm{Rad}}/(k_{0,\mathrm{Rad}} + k_{0,\mathrm{Mol}})$ at 2000 K, the present work has modeled $k_{0,\mathrm{Mol}}$ and $k_{0,\mathrm{Rad}}$ over the temperature range 1400−3200 K. Within the uncertainties of the now well-characterized experiments from refs 13−19 and the input molecular parameters, quite satisfactory agreement between experiment and theory was obtained. Equations 29−32 summarize our predictions for $k_{0,\mathrm{Mol}}$ and $k_{0,\mathrm{Rad}}$. Much cruder estimates for $k_{\infty,\mathrm{Mol}}$ and $k_{\infty,\mathrm{Rad}}$ have been also performed; see eqs 38 and 39. These values, however, still depend on uncertainties in the modeled specific rate constants $k_i(E)$. Experimental validations from high-pressure pyrolysis experiments are still lacking.

Our present analysis of the thermal dissociation practically rules out the suggestion from ref 25 of a lower value of the threshold energy $E_{0,1}/\mathrm{hc} = 27\,700\ \mathrm{cm}^{-1}$ and of a kinetic relevance of 6 times larger measured level densities than that expected. Instead, the present conclusions are essentially in line with the ab initio calculations of $E_{0,1}$ from ref 44 and the corresponding implications on level densities made in this reference.

The modeling of this work showed that collisional channel coupling, rotational channel switching, and channel branching above the threshold for radical formation in this reaction are superimposed in a well-characterized way and all have their specific kinetic relevance. The formaldehyde system with this study appears to be the best documented thermal multichannel dissociation reaction in its low-pressure range. Other systems such as the dissociations $C_2H_4 \rightarrow C_2H_2 + H_2/C_2H_3 + H$ or $C_3H_7I \rightarrow C_3H_6 + HI/C_3H_7 + I$ are expected to show analogous kinetic properties.

**Acknowledgment.** Discussions of the formaldehyde system with Th. Just, L. B. Harding, C. B. Moore, and P. Van Tiggelen over a long stretch of time have helped to finally unravel the described complexities of the kinetics. Thanks also go to J. M. Bowman who directed attention to ref 39 which appeared after submission of this article and stimulated an improved account for channel 3 in the final version of this article. Financial support of this work by the Deutsche Forschungsgemeinschaft (SFB 357 "Molekulare Mechanismen Unimolekularer Prozesse") is also gratefully acknowledged.

## Appendix: Modeling Parameters

**$H_2CO$.** Fundamental frequencies[54] $\omega_i^o/\mathrm{cm}^{-1} = 2811.42$, 1755.858, 1500.32, 1170.224, 2861.30, 1250.565. Rotational constants[40] $A = 9.405\ \mathrm{cm}^{-1}$, $B = 1.295\ \mathrm{cm}^{-1}$, $C = 1.134\ \mathrm{cm}^{-1}$.

**$H_2CO^{\ddagger}$ (channel 1).** Ab initio harmonic frequencies[43] $\omega_i^{\ddagger}/\mathrm{cm}^{-1} = 1840i$, 744, 833, 1246, 1835, 3127. Rotational constants[40,46] $A^{\ddagger} = 8.57\ \mathrm{cm}^{-1}$, $B^{\ddagger} = 1.20\ \mathrm{cm}^{-1}$, $C^{\ddagger} = 1.04\ \mathrm{cm}^{-1}$. $E_{o,1}/\mathrm{hc}\ \mathrm{cm}^{-1} = 28\,645$ (±105) from ref 44, 28 400 (±300) from this work.

**$H_2CO \rightarrow H + HCO$.** Fundamental frequencies[55] of HCO $\omega_i/\mathrm{cm}^{-1} = 1081$, 1868, 2435. $E_{0,2}/\mathrm{hc}\ \mathrm{cm}^{-1} = 30328.5$ (±0.5) from ref 27. Morse potential for H···CHO bond $D/\mathrm{hc}\ \mathrm{cm}^{-1} = 33\,310$, $r_e = 0.114$ nm, $\beta = 21.2\ \mathrm{nm}^{-1}$ (constructed from Figure 7 of ref 43).

**Collisional Parameters.** $\sigma_{\mathrm{LJ}}$ ($H_2CO$) ≈ 0.4 nm (estimated), $\epsilon_{\mathrm{LJ}}/\mathrm{k}$ ($H_2CO$) ≈ 400 K (estimated); $\sigma_{\mathrm{LJ}}$ (Ar) = 0.3542 nm, $\epsilon_{\mathrm{LJ}}/\mathrm{k}$ (Ar) = 93.3 K; $\sigma_{\mathrm{LJ}}$(Kr) = 0.36 nm, $\epsilon_{\mathrm{LJ}}/\mathrm{k}$(Kr) = 173 K.

**Vibrational Density of States.** $\rho_{\mathrm{vib,h}}(E_{0,1}) = 12.6/\mathrm{hc}\ \mathrm{cm}^{-1}$, $\rho_{\mathrm{vib,h}}(E_{0,2}) = 16.0/\mathrm{hc}\ \mathrm{cm}^{-1}$, Whitten−Rabinovitch factor[45] $a(E_{0,1}) = 0.975$, $a(E_{0,2}) = 0.976$.

**Anharmonicity Factor.** $F_{\mathrm{anh}}(E) \approx 1 + 0.89[(E + E_z)/(E_{0,1} + E_z)]^3$ with $E_z/\mathrm{hc} = 5873\ \mathrm{cm}^{-1}$ for $E \le E_{0,2}$, derived with the empirical method from ref 56 assuming that $\rho_{\mathrm{vib,h}}(E)$ is calculated with the fundamental (not harmonized) frequencies of $H_2CO$ from ref 54. The empirical method gives fair agreement with extrapolations (from the range $0 < E/\mathrm{hc} < 10\,000\ \mathrm{cm}^{-1}$) of anharmonic densities of states based on spectroscopic constants.[54] $F_{\mathrm{anh}}$ ($E/\mathrm{hc} = 27\,700\ \mathrm{cm}^{-1}$) ≈ 1 + 0.67 was estimated in ref 25 while the above expression gives $F_{\mathrm{anh}}$ ($E/\mathrm{hc} = 27\,700\ \mathrm{cm}^{-1}$) ≈ 1 + 0.82.

**Rotational Factors $F_{\mathrm{rot}}$.** For $T/\mathrm{K} = 1400$, 1700, 2000, 2500, and 3200 K, one has $F_{\mathrm{rot}} \approx 8.1$, 7.2, 6.2, 4.8, and 3.5, respectively.

**Density-of-States Factors $F_{\mathrm{E}}$.** For $T/\mathrm{K} = 1600$, 2000, 2400, and 2800 K one has $F_{\mathrm{E}}$ (channel 1) = 1.15, 1.20, 1.28, and 1.34 or $F_{\mathrm{E}}$ (channel 2) = 1.17, 1.22, 1.28, and 1.34, respectively.

## References and Notes

(1) Troe, J. *J. Chem. Soc., Faraday Trans.* **1994**, *90*, 2303.
(2) Troe, J. *J. Chem. Phys.* **1977**, *66*, 4745.
(3) Hold, U.; Lenzer, T.; Luther, K.; Symonds, A. C. *J. Chem. Phys.* **2003**, *119*, 11192.
(4) Lenzer, T.; Luther, K.; Reihs, K.; Symonds, A. C. *J. Chem. Phys.* **2000**, *112*, 4090. Fay, N.; Luther, K. *Z. Phys. Chem.* **2000**, *214*, 839.
(5) Grigoleit, U.; Lenzer, T.; Luther, K.; Mützel, M.; Takahara, A. *Phys. Chem. Chem. Phys.* **2001**, *3*, 2191.
(6) Lenzer, T.; Luther, K. *Phys. Chem. Chem. Phys.* **2004**, *6*, 955.
(7) Just, T.; Troe, J. *J. Phys. Chem.* **1980**, *84*, 3068 (part 1 of this series).

(8) Baulch, D. L.; Cobos, C. J.; Cox, R. A.; Esser, C.; Frank, P.; Just, T.; Kerr, J. A.; Pilling, M. J.; Troe, J.; Walker, R. W.; Warnatz, J. *J. Phys. Chem. Ref. Data* **1992**, *21*, 411.
(9) Baulch, D. L.; Bowman, C. T.; Cobos, C. J.; Cox, R. A.; Just, T.; Kerr, J. A.; Pilling, M. J.; Stocker, D.; Troe, J.; Tsang, W.; Walker, R. W.; Warnatz, J. *J. Phys. Chem. Ref. Data* **2005**, in press.
(10) Bhaskaran, K. A.; Frank, P.; Just, T. *Proceedings of the 12th International Symposium of Shock Tubes and Waves*; Jerusalem, Israel, 1979; p 503.
(11) Dean, A. M.; Craig, B. L.; Johnson, R. L.; Schultz, M. C.; Wang, E. E. *Proc. Combust. Inst.* **1979**, *17*, 577.
(12) Dean, A. M.; Johnson, R. L.; Steiner, D. C. *Combust. Flame* **1980**, *37*, 41.
(13) Saito, K.; Kakumoto, T.; Nakanishi, Y.; Imamura, A. *J. Phys. Chem.* **1985**, *89*, 3109.
(14) Rimpel, G.; Just, T. Unpublished data presented in ref 8.
(15) Irdam, E. A.; Kiefer, J. H.; Harding, L. B.; Wagner, A. F. *Int. J. Chem. Kinet.* **1993**, *25*, 285.
(16) Hidaka, Y.; Taniguchi, T.; Tanaka, H.; Kamesawa, T.; Inami, K.; Kawano, H. *Combust. Flame* **1993**, *92*, 365.
(17) Kumaran, S. S.; Carroll, J. J.; Michael, J. V. *Proc. Combust. Inst.* **1998**, *27*, 125.
(18) Eiteneer, B.; Yu, C.-L.; Goldenberg, M.; Frenklach, M. *J. Phys. Chem. A* **1998**, *102*, 5196.
(19) Friedrichs, G.; Davidson, D. F.; Hanson, R. K. *Int. J. Chem. Kinet.* **2004**, *36*, 157.
(20) Schecker, H. G.; Jost, W. *Ber. Bunsen-Ges.* **1969**, *73*, 521.
(21) Gay, I. D.; Glass, G. P.; Kistiakowsky, G.; Niki, H. *J. Chem. Phys*. **1965**, *43*, 4017.
(22) Buxton, J. P.; Simpson, C. J. S. M. *Chem. Phys. Lett.* **1986**, *128*, 577.
(23) Green, W. H.; Moore, C. B.; Polik, W. F. *Annu. Rev. Phys. Chem.* **1992**, *43*, 591 (and earlier references therein).
(24) Chuang, M.; Foltz, M. F.; Moore, C. B. *J. Chem. Phys.* **1987**, *87*, 3855.
(25) Polik, W. F.; Guyer, D. R.; Moore, C. B. *J. Chem. Phys.* **1990**, *92*, 3453.
(26) Van Zee, R. D.; Foltz, M. F.; Moore, C. B. *J. Chem. Phys.* **1993**, *99*, 1664.
(27) Terentis, A. C.; Kable, S. H. *Chem. Phys. Lett.* **1996**, *258*, 626.
(28) Valachovic, L. R.; Tuchler, M. F.; Dulligan, M.; Droz-Georget, T.; Zyrianov, M.; Kolessov, A.; Reisler, H.; Wittig, C. *J. Chem. Phys.* **2000**, *112*, 2752.
(29) Townsend, D.; Lahankar, S. A.; Lee, S. K.; Chambreau, S. D.; Suits, A. G.; Zhang, X.; Rheinecker, J.; Harding, L. B.; Bowman, J. M. *Science* **2004**, *306*, 1158.
(30) Yin, H.-M.; Nauta, K.; Kable, S. H. *J. Chem. Phys.* **2005**, *122*, 194312.
(31) Ho, P.; Bamford, D. J.; Buss, R. J.; Lee, Y. T.; Moore, C. B. *J. Chem. Phys.* **1982**, *76*, 3630.
(32) Moortgat, G. K.; Seiler, W.; Warneck, P. *J. Chem. Phys.* **1983**, *78*, 1185.
(33) Moortat, G. K.; Warneck, P. *J. Chem. Phys.* **1979**, *70*, 3639.
(34) Smith, G. D.; Molina, L. T.; Molina, M. J. *J. Phys. Chem. A* **2002**, *106*, 1233.
(35) Pope, F. D.; Smith, C. A.; Davis, P. R.; Shallcross, D. E.; Ashfold, M. N. R.; Orr-Ewing, A. J. *Faraday Discuss. Chem. Soc.* **2005**, *130*, 000.
(36) Atkinson, R.; Baulch, D. L.; Cox, R. A.; Hampson, R. F.; Kerr, J. A.; Rossi, M. J.; Troe, J. *J. Phys. Chem. Ref. Data* **1999**, *28*, 191.
(37) Atkinson, R.; Baulch, D. L.; Cox, R. A.; Crowley, J. N.; Hampson, R. F.; Rossi, M. J.; Troe, J. http://www.iupac-kinetic.ch.cam.ac,uk/2002, P1.
(38) Sander, S. P.; Friedl, R. R.; Golden, D. M.; Kurylo, M. J.; Huie, R. E.; Orkin, V. L.; Moortgat, G. K.; Ravishankara, A. R.; Kolb, C. E.; Molina, M. J.; Finlayson-Pitts, B. J. *JPL Publ.* **2003**, *02*−*25*, 4−21.
(39) Zhang, X.; Rheinecker, J. L.; Bowman, J. M. *J. Chem. Phys.* **2005**, *122*, 114313.
(40) Goddard, J. D.; Schaefer, H. F. *J. Chem. Phys.* **1979**, *70*, 5117.
(41) Gray, S. K.; Miller, W. H.; Yamaguchi, Y.; Schaefer, H. F. *J. Am. Chem. Soc.* **1981**, *103*, 1900.
(42) Yamaguchi, Y.; Wesolowski, S. S.; Van Huis, T. J.; Schaefer, H. F. *J. Chem. Phys.* **1998**, *108*, 5281.
(43) Zhang, X.; Zou, S.; Harding, L. B.; Bowman, J. M. *J. Phys. Chem. A* **2004**, *108*, 8980.
(44) Feller, D.; Dupuis, M.; Garrett, B. C. *J. Chem. Phys.* **2000**, *113*, 218.
(45) Forst, W. *J. Phys. Chem.* **1983**, *87*, 4489, 5234.
(46) Troe, J. *J. Phys. Chem.* **1984**, *88*, 4375.
(47) Bauerfeld, G. F.; de Albuquerque, L. M. M.; Arbilla, G.; Da Silva, E. C. *J. Mol. Struct. (THEOCHEM)* **2002**, *580*, 147.
(48) Troe, J. To be submitted for publication, 2005.
(49) Troe, J. *J. Chem. Phys.* **1977**, *66*, 4758.
(50) Troe, J. *J. Phys. Chem.* **1979**, *83*, 114.
(51) Troe, J. *Proc. Combust. Inst.* **2000**, *28*, 1463.
(52) Cobos, C. J.; Troe, J. *Z. Phys. Chem.* **1992**, *176*, 161.
(53) Chase, M. W. NIST-JANAF Thermochemical Tables, *J. Phys. Chem. Ref. Data*, *Monograph 9*, 1998.
(54) Reisner, D. E.; Field, R. W.; Kinsey, J. L.; Dai, H. L. *J. Chem. Phys.* **1984**, *80*, 5968.
(55) Tobiason, J. D.; Dunlop, J. R.; Rohlfing, E. A. *J. Chem. Phys.* **1995**, *103*, 1448.
(56) Troe, J. *Chem. Phys.* **1995**, *190*, 381.